

CHANDRA X-RAY OBSERVATIONS OF THE YOUNG OPEN CLUSTER NGC 2516

F. DAMIANI, E. FLACCOMIO, G. MICELA, AND S. SCIORTINO

INAF, Osservatorio Astronomico di Palermo G. S. Vaiana, Piazza del Parlamento 1, I-90134 Palermo, Italy;
damiani@oapa.astropa.unipa.it, ettoref@oapa.astropa.unipa.it, giusi@oapa.astropa.unipa.it, sciorti@oapa.astropa.unipa.it

F. R. HARNDEN, JR., S. S. MURRAY, AND S. J. WOLK

Smithsonian Astrophysical Observatory, 60 Garden Street, Cambridge, MA 02138;
frh@cfa.harvard.edu, ssm@cfa.harvard.edu, swolk@cfa.harvard.edu

AND

R. D. JEFFRIES

Department of Physics, Keele University, Keele, Staffordshire ST5 5BG, UK; rdj@astro.keele.ac.uk

Received 2002 September 16; accepted 2003 January 15

ABSTRACT

We present a comprehensive study of the *Chandra* X-ray observations of the young open cluster NGC 2516. We have analyzed eight individual *Chandra* observations. We have combined the data to achieve the greatest sensitivity, reaching down to $\log f_X = -14.56$ (ergs $s^{-1} cm^{-2}$), or $\log L_X = 28.69$ (ergs s^{-1}) at the distance of NGC 2516. Out of 284 X-ray sources detected, 155 are identified with photometric cluster members, with very little ambiguity. We have studied the X-ray luminosity functions for the various spectral types, correcting for nonmember contamination those for later type stars. We find strong X-ray emission from a couple of B stars that cannot be due to companions. Among A stars, chemically peculiar stars show a detection fraction much larger than normal A stars. The luminosity functions decrease monotonically from F to M stars, and those for K stars are significantly lower than similar stars in the Pleiades, a cluster only slightly younger than NGC 2516. We discuss possible causes of this discrepancy, including differences in age and stellar rotation.

Subject headings: open clusters and associations: individual (NGC 2516) — stars: coronae — X-rays: stars

On-line material: machine-readable tables

1. INTRODUCTION

The young southern open cluster NGC 2516 has been studied with increased interest in the last decade. It bears many similarities with the well-studied Pleiades cluster; however, it differs in some nonnegligible respects. NGC 2516 is only slightly older than the Pleiades: Mermilliod (1981) estimates its age as 107 Myr, to be compared with 78 Myr of the Pleiades. Other authors (e.g., Snowden 1975) give a different age estimate but about the same relative age with respect to the Pleiades. However, it appears to contain many more stars than the Pleiades, of both high mass (Dachs 1970) and low mass (Jeffries et al. 2001). There are various estimates of its distance modulus, most of which are in agreement with the value 7.94, or $d = 387$ pc, given by Jeffries et al. (1997), which will be adopted here. The *Hipparcos* data yield for NGC 2516 a distance of $d = 346.0^{+27.1}_{-23.4}$ pc (Robichon et al. 1999), in agreement within 1.5σ with the Jeffries et al. value.

Unlike the Pleiades, NGC 2516 contains a few chemically peculiar Ap stars (Dachs 1970). However, spectra exist only for the brighter cluster members, while for most putative members they are still lacking. This is especially unfortunate since in recent years doubts have arisen about the chemical composition of the cluster stars. Jeffries et al. (2001 and references therein) have found on the basis of photometric data, a probable metal underabundance by a factor of 2 with respect to the Sun (and to the Pleiades). Analogous results by other authors seem to lead to a consensus that this is actually the case. However, in a more recent work, Terndrup et al. (2002) find a solar-like metal abundance for NGC 2516, on the basis of high-resolution spectra.

NGC 2516 has also been studied in X-rays with *ROSAT*, using both the Position Sensitive Proportional Counter (PSPC; Dachs & Hummel 1996; Jeffries et al. 1997), and the High Resolution Imager (HRI; Micela et al. 2000). Based on the optical member lists available at that time, some differences were already found in the NGC 2516 X-ray luminosity functions with respect to Pleiades stars. In particular, the G and K stars in NGC 2516 were found to be underactive in X-rays with respect to the Pleiades G and K stars, while no such difference was found for M stars. Jeffries et al. (1997) thoroughly discuss how these differences could be related to a low-metallicity effect, through a different evolution of the stellar internal structure. In light of the new high-resolution optical data, these explanations cannot hold any more. Our purpose here is to first ascertain, on the basis of the new, higher quality X-ray data made available using *Chandra*, if differences with respect to the Pleiades X-ray emission persist and then to obtain clues about the origin of any peculiarity of the X-ray emission of NGC 2516. A preliminary analysis was made by Harnden et al. (2001), using a subset of the *Chandra* data that we study in this work. NGC 2516 was also observed with *XMM-Newton*, and the analysis of two observation segments was made by Sciortino et al. (2001). The analysis of additional segments is underway (I. Pillitteri et al. 2003, in preparation).

The larger distance of NGC 2516 with respect to the Pleiades requires that proportionally more sensitive X-ray observations are needed to study the two clusters with comparable detail. Moreover, the apparent X-ray source density is also larger in NGC 2516, which makes high spatial resolution highly desirable, especially in order to obtain unambiguous X-ray-optical identifications. As we will see in § 4, the

TABLE 1
OBSERVATION JOURNAL FOR NGC 2516

ObsID	R.A. (J2000)	Decl. (J2000)	Date	Detector	Raw T_{exp} (s)	Raw Events	Screened T_{exp} (s)	Screened Events
66.....	7 58 05.6	-60 45 19.7	1999 Aug 22	ACIS-S	11914.34	628,199	9904.96	244,768
1229	7 58 05.6	-60 45 19.7	1999 Aug 22	ACIS-S	10930.38	556,535	10930.38	205,524
65.....	7 58 20.1	-60 47 20.4	1999 Aug 26	ACIS-I	20155.78	723,201	9901.81	109,006
1232	7 58 20.1	-60 47 20.3	1999 Aug 27	ACIS-I	10685.11	1,807,826	8499.00	740,878
1405	7 58 08.3	-60 45 21.1	1999 Oct 25	HRC-I	20304.46	1,012,792	20204.56	531,202
1458	7 58 16.8	-60 54 59.2	1999 Nov 02	ACIS ^a	11585.49	474,787	9652.21	26,606
27.....	7 58 08.5	-60 45 50.1	2000 Feb 15	HRC-I	49303.32	3,105,919	42156.83	1,243,781
999.....	7 58 20.0	-60 46 22.4	2001 Mar 05	HRC-I	18088.14	837,823	18076.93	451,524

NOTE.—Units of right ascension are hours, minutes, and seconds, and units of declination are degrees, arcminutes, and arcseconds.

^a Used a nonstandard choice of chips: 2, 3, 6, 7, and 8.

Chandra data analyzed here are almost ideal in this respect. By comparison, the *XMM-Newton* data become increasingly confused near the cluster center, as the limiting sensitivity goes deeper.

2. CHANDRA DATA ON NGC 2516

NGC 2516 has been observed by *Chandra* with all its detectors in imaging mode, three times with the HRC-I, once with the HRC-S, twice with ACIS-I, twice with ACIS-S, and once with a nonstandard ACIS chip configuration. The HRC-S observation contains little new information and presents special difficulties for its analysis; therefore, it has not been considered in this work. Therefore, we have analyzed eight individual pointings, whose details are reported in Table 1. The deep HRC-I observation Observation ID (ObsID) 27 was part of the HRC-team GTO observation program, while all other pointings were taken as calibration data sets to determine accurate bore-sight corrections for all imaging detectors, due to the availability of a number of moderately bright point sources over a suitable sky area.

The target coordinates of all NGC 2516 pointings (except for ObsID 1458) lie within 2' from one another, and from cluster center. ObsID 1458 was targeted 9.5' southward, but there is still a large overlap between its field of view and those of all other ObsIDs.

We recall briefly some properties of the relevant *Chandra* instruments used in this work. HRC-I is a microchannel plate, covering 32' \times 32' on the sky, with 0''.127 pixels that adequately sample the on-axis *Chandra* point-spread function (PSF; 0''.5 FWHM). While its intrinsic sensitivity is rather uniform, its true sensitivity is dominated by telescope vignetting and off-axis widening of the PSF. ACIS-I is a smaller (16' \times 16') but more sensitive CCD-mosaic detector, made of 2 \times 2 front-illuminated (FI) chips. ACIS-S is instead a linear array (8' \times 48') of six CCDs, alternating front-illuminated and back-illuminated (BI) chips. Since FI and BI chips have different properties (sensitivity, background level), this poses special problems in the analysis of ACIS-S images. Moreover, all ACIS CCDs can be operated independently, and any choice of up to six chips is, in principle, possible, allowing nonstandard configurations such as ObsID 1458, where chips 2, 3, 6, 7, and 8 were used. The ACIS pixel size is 0''.5 and therefore undersamples the on-axis *Chandra* PSF. HRC allows accurate timing of recorded X-ray events but has no spectral resolution. On the con-

trary, the standard ACIS observing mode (as in our case) yields a time resolution of only about 3.2 s but gives moderate ($R \sim 35$ –50) resolution spectral information.

The fields of view of all *Chandra* pointings used in this work are shown in Figure 1, overlaid on the optical Digitized Sky Survey (DSS) red image of NGC 2516.

3. X-RAY DATA ANALYSIS

We have first analyzed separately each of the eight NGC 2516 *Chandra* observations to derive lists of detected sources with their X-ray fluxes and apparent sizes. Then we have taken advantage of the rather unique opportunity offered by the large overlap of these observations to achieve a deeper sensitivity by combining many pointings together, as we explain in detail in § 3.2.

Before starting analysis, we “cleaned” our data, removing known hot pixels and bad columns. To reject most non-X-ray events we have selected ACIS events with grades = 0, 2, 3, 4, and 6 in the energy band 0.3–8.0 keV. For HRC-I, we have selected photons in the pulse-height amplitude (PHA) range 35–600, since outside of this range one only finds non-X-ray events. Moreover, we have developed a method to maximize the signal-to-noise ratio (S/N) of weak sources, screening out time intervals with high background level. These occur occasionally, especially because of eruptive solar events, and on timescales typically shorter than the length of an individual *Chandra* observation; they are sometimes very evident in the background light curve of an observation. It can be shown that by rejecting all photons recorded when the background level is higher than a certain threshold, the S/N of weak sources reaches a maximum, usually larger than if no rejection is made. We have therefore computed the background threshold relative to each of our observations and discarded all time intervals with higher background.

In Table 1 we list for each pointing its raw exposure time and number of events (as in Level 1 processed data) and the exposure time and number of events after screening. In some cases, the amount of time rejected because of high background is substantial, and in these instances our screening permits a dramatic improvement in the S/N of weak sources.

For each data set, we have computed an exposure map (using the CIAO task “mkexpmap”), using spectral weights appropriate to a thermal MEKAL model with temperature 0.5 keV and absorption $N_{\text{H}} = 7.0 \times 10^{20} \text{ cm}^{-2}$, to

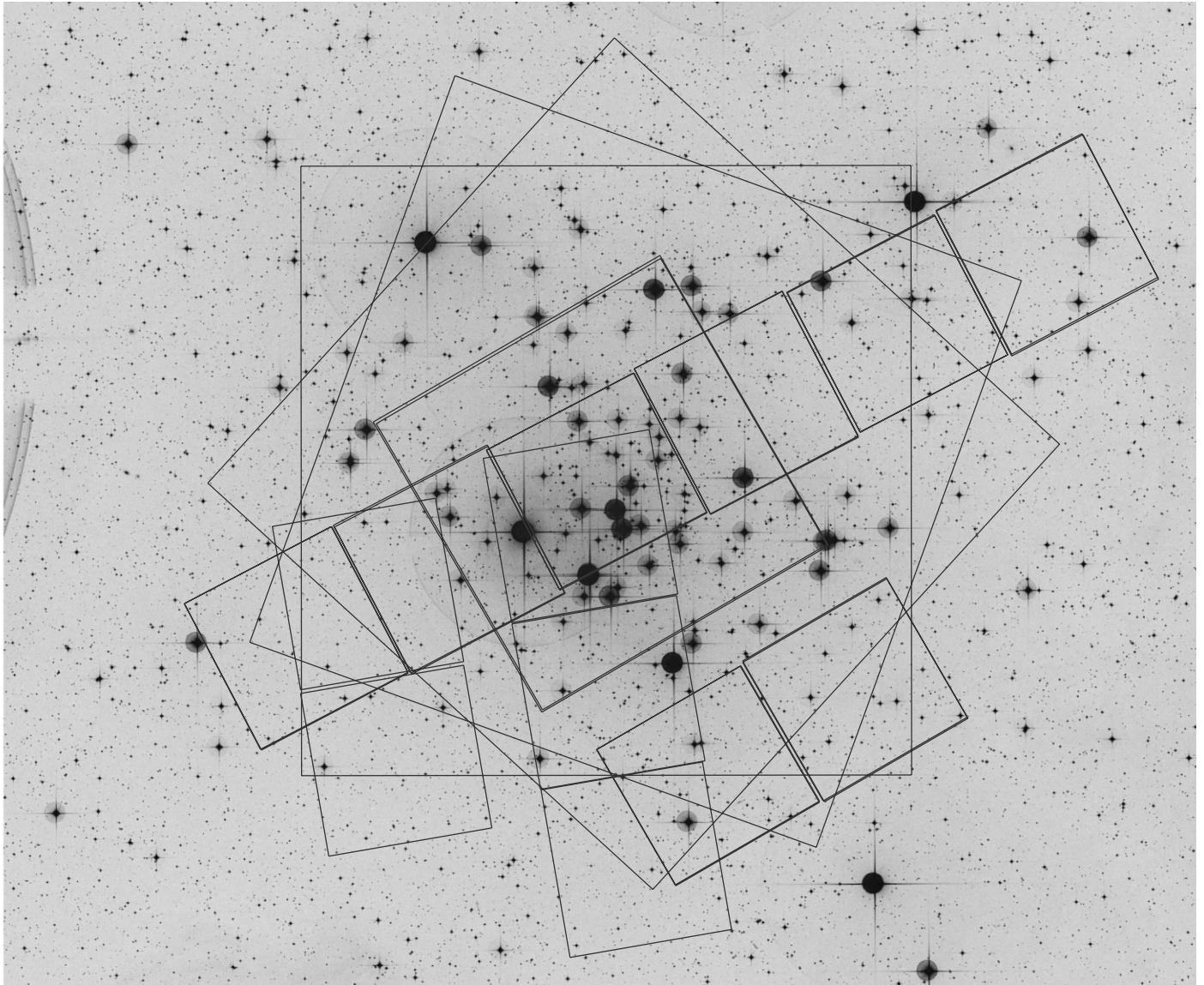


FIG. 1.—Optical DSS image of NGC 2516, with indicated fields of view of all *Chandra* pointings considered in this work. Large squares: HRC-I; intermediate squares: ACIS-I; small squares: single ACIS chips. North is up, and east is to the left.

mimic the spectrum expected for X-ray sources in our cluster. For ACIS-S, separate exposure maps were computed for FI and BI chips, respectively, since they have markedly different sensitivities.

3.1. Individual Pointings

Source detection was performed for each individual data set using “PW Detect,” a wavelet-transform detection algorithm recently developed at the Osservatorio Astronomico di Palermo (F. Damiani et al. 2003, in preparation), based on its *ROSAT* predecessor called “WDetect” (Damiani et al. 1997a, 1997b).¹ Like other wavelet-based detection methods, it performs a multiscale search for sources, that can range from pointlike up to 0.3 or more. The main features of PW Detect are the following:

1. It works directly on (unbinned) event lists, that permits a complete exploration of the spatial information contained in *Chandra* observations, without the inefficiency intrinsic to huge full-resolution images, nor the spatial degradation of rebinned images.

2. It uses exposure maps to correct for underexposed regions (e.g., ACIS gaps) and to derive accurate source fluxes.

3. It computes reference maps of the background that take into account its strictly Poisson statistics, and are accurate even in the limit of very low background (per resolution element), minimizing the effect of nearby point sources.

4. It has been extensively tested on large sets of pure-background *Chandra* simulations, from which were derived the appropriate thresholds to obtain a desired number of spurious detections per field.

Since the actual *Chandra* PSF is not Gaussian, as assumed by PW Detect, we needed to apply a correction factor to the detected source count rates. This factor was derived by computing the wavelet transform of the

¹ PW Detect is now available publicly at the address http://www.astropa.unipa.it/progetti_ricerca/PWDetect/.

TABLE 2
NUMBER OF DETECTIONS AND SENSITIVITY FOR INDIVIDUAL NGC 2516 POINTINGS

ObsID	NUMBER OF DETECTIONS							LOWEST DETECTED FLUX (counts s ⁻¹ cm ⁻²)	
	HRC-I	ACIS-I	ACIS CCD_ID				Total		
			2	3	5	6			
66.....					1	30	35	66	1.46×10^{-6}
1229.....					0	29	34	63	1.32×10^{-6}
65.....		126				3	1	130	1.81×10^{-6}
1232.....		72				0	1	73	2.48×10^{-6}
1405.....	80							80	1.57×10^{-6}
1458.....			5	5			35	43	0.96×10^{-6}
27.....		116						116	0.94×10^{-6}
999.....		74						74	2.10×10^{-6}

calibration PSFs at different positions across the field of view, separately for each *Chandra* detector. This amounted to a count-rate correction of up to 30% near the center, and more typically 10%–15%, for a representative energy of 1.4967 keV. From a study of the HRC image of Orion Trapezium (Flaccomio et al. 2003), we have learned that the HRC calibration PSFs need first to be convolved with a Gaussian with $\sigma = 0''.3$. The same study has also shown that the maximum positional error due to PSF distortion is 0''.8 for off-axis angles up to 10', and 1''.5 across the whole field of view.

For this work, we use a modified version of PWDetect, that also computes upper limits for undetected objects. We compute upper limits for all NGC 2516 candidate members from optical photometry listed by Jeffries et al. (2001; see § 4), plus brighter members listed by Jeffries et al. (1997). The optical survey of Jeffries et al. (2001) covers completely the spatial region of our X-ray study. To these optical star positions, we have added X-ray source positions detected in at least one of our *Chandra* pointings of NGC 2516. The same PSF-related correction factor was applied to the upper limit count rates computed by PWDetect.

We have chosen for each pointing a threshold corresponding to one spurious detection per field. Since the integrated background varies from one data set to another, the threshold varies accordingly. After running PWDetect, the detected source list for each data set was carefully checked for possible “double” detections, namely, X-ray sources that PWDetect splits each in two detections, since it is misled by the elongated off-axis PSF shape. The effect of this strongly noncircular PSF on the detection procedure is difficult to correct in general terms, and we have found it more convenient to clean the PWDetect source lists afterward. Visually, these double detections are easily recognized since all detection pairs in the same neighborhood are oriented nearly in the same direction, following the PSF elongation. To do this cleaning more automatically, we have found that a good rule for our NGC 2516 fields is to merge into one source all pairs with separation $d < 2\Delta r$ (where Δr is the PWDetect computed positional error) or $d < 3''.5$. This latter term accounts for the PSF distortion. Only one source pair (in ObsID 1458) not satisfying these conditions appears to be real and has therefore been retained in the final source list. All detections are pointlike sources.

In ACIS-S data sets, there are adjacent FI and BI chips, with very different background levels. These were analyzed separately with PWDetect, and the resulting source lists

merged. No sources were detected in ACIS-S chips 4 and 9. Chip 8 is affected by severe instrumental noise (streaks), and although this may be corrected, it does not contain obvious sources in our observations. The PWDetect results for all individual NGC 2516 *Chandra* data sets, after cleaning, are summarized in Table 2. In the table, ACIS-I refers to chips 0123, analyzed together. When ACIS chips are analyzed individually, detections are listed in their respective columns.

3.2. Summed Pointings

The three HRC-I observations ObsIDs 27, 1405, and 999, and the two ACIS-I observations ObsIDs 65 and 1232 are pointed within 2' of one another, and their fields of view are homogeneous (no FI-BI chips alternance). Therefore, we have modified our PWDetect code in a way to enable it to detect sources in a combined data set, comprising all photons of the three HRC-I and two ACIS-I data sets just mentioned. Of course, this has also required the combining of the individual exposure maps of all input data sets, built as explained in the previous section.

Combining event lists (or images) pertaining to detectors with different properties is not trivial. We have chosen to combine only data sets without strong discontinuities inside them. We have also made certain that the pointing is nearly the same, so that the PSF does not change very much from one to another (the *Chandra* PSF is essentially constant within a radius of about 4' from center and varies sufficiently slowly outside 4'). Finally, to derive meaningful source fluxes one has to use exposure maps in “physical units,” i.e., not just time, but time cm². In this way we can combine data sets obtained with HRC-I and with ACIS-I (whose effective areas differ by about a factor of 3) and still derive reliable source fluxes.

Another matter of concern is whether residual errors in the *Chandra* aspect reconstruction between different observations exist, as they need to be corrected before combining data sets. We have evaluated these shifts as median offsets between matching detections in different data sets, and they turn out to be at most about 0''.35, enough to distort significantly the on-axis PSF. We have therefore shifted each input event list accordingly (with respect to the mean position of all data sets).

Using the upgraded PWDetect, we detect 189 sources in the combined (three HRC-I + two ACIS-I) data set, with only one spurious expected, with the lowest detection

having a photon flux of 0.76×10^{-6} counts $\text{s}^{-1} \text{cm}^{-2}$. Since these sources may be variable, they can occasionally be detected in shorter time segments, but not in a longer observation where the background is larger. Therefore, we have also considered the sum of the three HRC-I data sets, and the sum of the two ACIS-I, where we indeed detect one and 16 sources, respectively, not detected in the “all-summed” data set. Our “combined-data set” source list therefore comprises 206 individual X-ray detections.

The very deep *Chandra* image of NGC 2516, obtained from the sum of three HRC-I and two ACIS-I data sets, is shown in Figure 2. We note that had we included ACIS BI chips in this combined analysis we could not have obtained better results: these chips are characterized by a stronger background than the FI chips, that in the combined image would have hidden more sources than the possible new sources found due to the additional effective area.

3.3. Final X-Ray Source List

Having obtained detection lists for each data set separately, and another detection list for the combined one (plus the additional detections from the three HRC-I data sets

summed and the two ACIS-I data sets summed), we then combined them in a final detection list. The number of expected spurious detections is one per data set, and since they are statistically independent (all but the sums), the total number of spurious detections should be 8–9. In doing this merging, we have applied shifts to the source positions from each data set, computed as described in § 3.1.

A match between detections from different data sets was made whenever their distance was $d < 3\Delta r$ (where Δr is the PWDetect computed positional error). In some instances this resulted in multiple matches, and we have then retained only those with the smallest distance (the rejected matches having $d > 1.5\Delta r$).

The resulting final source list is reported in Table 3 and comprises 284 unique detections. We report photon fluxes for the individual data sets (including the all-summed data set) in units of 10^{-6} counts $\text{s}^{-1} \text{cm}^{-2}$, homogeneously for all detectors as explained. We include in the same table the flux upper limit for sources undetected in a particular data set. Entries in italics (either detections or upper limits) refer to sources falling in ACIS BI chips. Where an entry is missing the source fell outside the field of view of that particular data set. As seen in the table, in addition to the 206

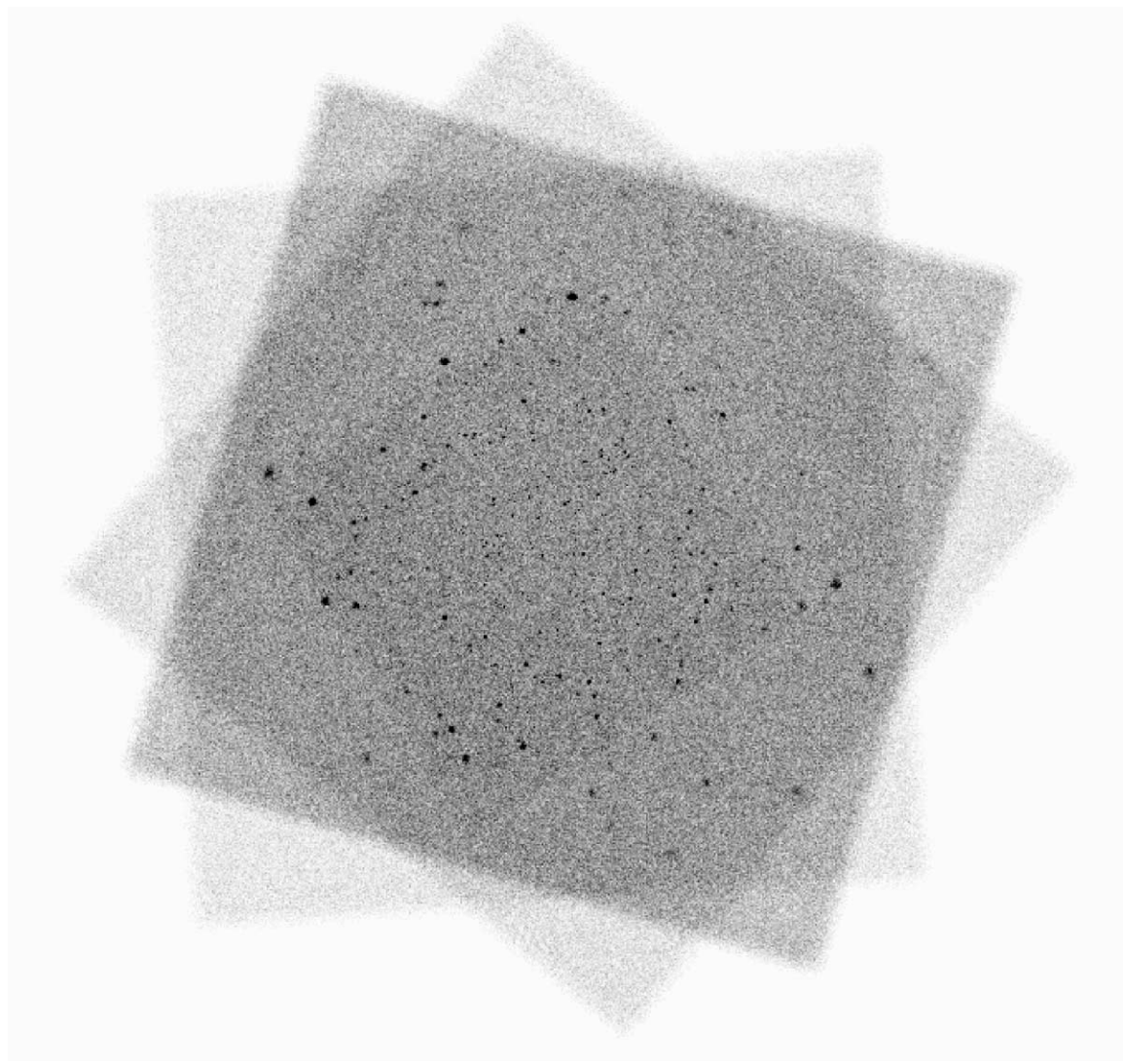


FIG. 2.—Combined *Chandra* X-ray image of NGC 2516, made using three HRC-I and two ACIS-I data sets. North is up, and east is to the left.

TABLE 3
NGC 2516 X-RAY SOURCE MATCHES

X-Ray Source Number	Flux3 HRC+2ACIS ^a	Flux HRC27	Flux HRC1405	Flux HRC999	Flux ACIS65 ^b	Flux ACIS1232 ^b	Flux ACIS1229 ^b	Flux ACIS66 ^b	Flux ACIS1458 ^b
1.....	40.50 ± 4.27	60.84 ± 6.36	<30.77	<37.37	19.93 ± 5.89	<37.33
2.....	40.13 ± 4.15	33.97 ± 5.25	55.44 ± 10.09	53.77 ± 9.13
3.....	12.17 ± 1.88	14.80 ± 3.73	18.67 ± 5.55	<21.17	11.71 ± 3.83	<18.91
4.....	6.54 ± 1.74	7.51 ± 2.25	<15.20	<21.10	11.07 ± 3.41	15.21 ± 4.14	...
5.....	24.48 ± 4.13	<24.65	43.46 ± 7.93	<38.84	48.51 ± 7.36	<41.19
6.....	15.87 ± 2.05	14.58 ± 2.69	20.74 ± 5.46	22.87 ± 6.45
7.....	4.47 ± 1.22	<9.56	<13.69	<17.08	<5.68	<10.87
8.....	20.08 ± 4.88	25.93 ± 6.60	<31.17	<36.45
9.....	13.26 ± 1.96	9.42 ± 2.41	13.13 ± 3.51	7.64 ± 2.72	16.58 ± 2.60	19.99 ± 2.99	...
10.....	4.14 ± 1.07	5.76 ± 1.69	7.66 ± 2.59	<9.75	<3.95	<7.99

NOTE.—Table 3 is published in its entirety in the electronic edition of the *Astrophysical Journal*. A portion is shown here for guidance regarding its form and content.

^a Units for fluxes and errors are 10^{-6} counts $s^{-1} cm^{-2}$. Effective areas are $194.8 cm^2$ for 3HRC+2ACIS, $174.7 cm^2$ for HRC, $286.6 cm^2$ for ACIS-I, and $531.3 cm^2$ for ACIS back-illuminated chips.

^b Fluxes in italics are for the back-illuminated ACIS S3 chip.

detections in the combined data set we find two more sources in ObsID 27 (HRC-I), one in ObsID 1405 (HRC-I), one in ObsID 999 (HRC-I), eight in ObsID 65 (ACIS-I), 11 in ObsID 1229 (ACIS-S), seven in ObsID 66 (ACIS-S), and 48 in ObsID 1458 (ACIS-23678). The large number of additional detections in ObsID 1458 arises largely because of its different pointing than the other data sets.

Table 3 forms the basis of a study of X-ray variability in NGC 2516 that will be the subject of a companion paper (S. J. Wolk et al. 2003, in preparation). For the rest of this work, however, we will use average source fluxes and positions. We have computed weighted averages of positions and fluxes for all sources detected more than once, using the inverse square of the error as weight. The detected source flux in the combined data set is itself a maximum-likelihood average, and it was further averaged with the flux in the data sets not in the combination (ObsIDs 66, 1229, and 1458), when a source is detected also in these latter. The average for sources not in the combined-data set list was made using detections in all data sets, but not including upper limits. However, including upper limits to compute a maximum-likelihood average flux would have changed little our

results, since in most cases they are well compatible with the detected flux values. The resulting mean source fluxes and positions are listed in Table 4. In many cases, the uncertainty on source position is a fraction of an arcsecond, thanks to the extremely narrow *Chandra* PSF.

3.4. X-Ray Source Fluxes

To convert X-ray count rates (or photon fluxes) to true fluxes, one needs to estimate a suitable conversion factor. Since the instrument effective area is already embodied in the derived photon fluxes, the conversion factor takes here the form of an “effective” photon energy. We have taken advantage of the availability of the ACIS spectra for many of our X-ray sources to estimate the spectral parameters of NGC 2516 stars. For all sources detected in ACIS FI chips, we have merged their extracted (background-subtracted) ACIS FI spectra to compute color ratios with the best statistics. We have chosen three bands to compute two color ratios, namely, 0.3–0.75, 0.75–1.5, and 1.5–8.0 keV. These were chosen with the purpose of maximizing the average number of counts in each band. We have defined

TABLE 4
NGC 2516 X-RAY SOURCE OPTICAL IDENTIFICATIONS

X-Ray Sources Number	Mean R.A.	Mean Decl.	Position Error (arcsec)	Flux (10^{-6} counts $s^{-1} cm^{-2}$)	Number of Detections	Star Number	Offset (arcsec)	<i>V</i>	<i>B-V</i>	<i>V-I</i>	Member Flag	Binary Flag
1.....	7 56 22.50	-60 51 42.2	5.20	40.50 ± 4.27	3	4103	4.01	11.787	0.305	0.801	No	Yes
	4125	1.25	11.556	0.513	0.659	Yes	Yes
2.....	7 56 34.56	-60 48 03.6	3.94	40.13 ± 4.15	4	4598	0.32	13.984	0.861	1.016	Yes	Yes
3.....	7 56 46.36	-60 48 58.6	2.79	12.17 ± 1.88	4	15496	0.31	8.360	0.020	...	Yes	No
4.....	7 56 46.88	-60 43 23.2	3.20	8.42 ± 2.33	4	5024	1.33	16.324	1.331	1.655	Yes	No
5.....	7 56 47.55	-60 56 48.9	6.06	24.48 ± 4.13	3	5052	2.32	10.854	0.344	0.452	Yes	Yes
6.....	7 56 48.08	-60 46 32.3	2.93	15.87 ± 2.05	4	5061	1.10	15.410	1.268	1.545	Yes	Yes
7.....	7 56 59.49	-60 49 57.4	2.63	4.47 ± 1.22	1	5447	0.64	16.555	1.348	1.912	No	Yes
8.....	7 57 11.72	-60 33 09.5	6.63	20.08 ± 4.88	2	5957	2.98	14.576	1.015	1.080	Yes	No
	5968	6.46	16.970	0.750	0.974	No	No
9.....	7 57 14.13	-60 40 52.6	1.77	15.65 ± 2.37	6	6029	0.15	12.240	0.674	0.769	Yes	Yes
10.....	7 57 16.42	-60 47 12.8	1.96	4.14 ± 1.07	3	6106	1.70	12.035	0.537	0.652	Yes	No

NOTE.—Table 4 is published in its entirety in the electronic edition of the *Astrophysical Journal*. A portion is shown here for guidance regarding its form and content. Units of right ascension are hours, minutes, and seconds, and units of declination are degrees, arcminutes, and arcseconds.

color ratios as $CR_1 = 2.5 \log[N_{\text{counts}}(0.75\text{--}1.5 \text{ keV})/N_{\text{counts}}(0.3\text{--}0.75 \text{ keV})]$ and $CR_2 = 2.5 \log[N_{\text{counts}}(1.5\text{--}8.0 \text{ keV})/N_{\text{counts}}(0.75\text{--}1.5 \text{ keV})]$.

Using PIMMS, we have computed, in the $CR_1 - CR_2$ plane, a grid corresponding to Raymond-Smith single-temperature thermal models, with solar abundances, with different temperatures in the range $\log T = 6.0\text{--}7.8$ [K], and absorption in the range $N_{\text{H}} = 1 \times 10^{20}$ to $5 \times 10^{21} \text{ cm}^{-2}$. We find clearly that our color ratios cannot be reproduced using these models, for any choice of temperature and absorption, as was found by Jeffries et al. (1997) using *ROSAT* PSPC data. We have therefore tried with two-temperature Raymond-Smith models, where we have two more parameters: the temperature of the second component and its relative normalization. To reduce the parameter space, we have fixed the absorption to the value $N_{\text{H}} = 8.2 \times 10^{20} \text{ cm}^{-2}$, corresponding to the cluster extinction $A_V = 0.372$ (Jeffries et al. 2001). Moreover, the first temperature was set to $\log T = 6.5$ [K], a value usually found in two-temperature models of coronal sources of the same age (e.g., in the Pleiades; Gagné, Caillault, & Stauffer 1995). Therefore, we have computed a grid analogous to the former but now having as variables the second temperature and the component intensity ratio. In this case we find that most observed color ratios can be well reproduced, especially those with the smallest errors, and those of cluster members better than nonmembers (we discuss the identification of X-ray sources in § 4). We have therefore adopted these two-temperature models to compute conversion factors for NGC 2516 coronal sources, using PIMMS.

In our sample there are 24 sources (among cluster members) with more than 50 counts in the combined ACIS FI spectra. Their position in the CR_1 - CR_2 plane is defined with small errors, and thus we have computed for each of them individually a (second) temperature and component ratio, and therefore a conversion factor. For the remaining weaker detections and for upper limits (§ 4), the conversion factor was chosen as the median conversion factor of the stronger sources with the same spectral type. The derived higher temperatures are in the range $\log T = 6.87\text{--}7.60$ [K], and the high-to-low temperature component input count ratios are in the range 0.098–2.88. The obtained conversion factors are in the range $(2.42\text{--}3.46) \times 10^{-9} \text{ ergs counts}^{-1}$. (average photon energies in the range 1.51–2.16 keV). Dividing this by the adopted ACIS-I spectrum-weighted on-axis effective area, we obtain the more usual count rate to flux conversion factor, in our case in the range $(8.46\text{--}12.1) \times 10^{-12} \text{ ergs cm}^{-2} \text{ counts}^{-1}$ for ACIS-I, in very good agreement with Harnden et al. (2001). This translates into a flux for our weakest detected X-ray source of $\log f_{\text{X}} = -14.56$ ($\text{ergs s}^{-1} \text{ cm}^{-2}$), in the band 0.1–4.0 keV, which corresponds to a minimum X-ray luminosity, at the distance of NGC 2516, of $\log L_{\text{X}} = 28.69$ (ergs s^{-1}). For nonmember detections, we have adopted a conversion factor of 1.8 keV, and the lowest detected flux is $\log f_{\text{X}} = -14.66$ ($\text{ergs s}^{-1} \text{ cm}^{-2}$). The minimum flux reached by Harnden et al. (2001) using a subset of these *Chandra* data was $\log f_{\text{X}} \sim -14.6$ ($\text{ergs s}^{-1} \text{ cm}^{-2}$), and about the same value was reached by Sciortino et al. (2001) using *XMM/Newton* data. Earlier *ROSAT* studies had reached instead $\log f_{\text{X}} \sim -14.25$ ($\text{ergs s}^{-1} \text{ cm}^{-2}$), or $\log L_{\text{X}} \sim 29.0$ (ergs s^{-1}) (Jeffries et al. 1997), and $\log f_{\text{X}} \sim -13.95$ ($\text{ergs s}^{-1} \text{ cm}^{-2}$), or $\log L_{\text{X}} \sim 29.3$ (ergs s^{-1} ; Micela et al. 2000). The derived X-ray luminosities for the detected NGC 2516

members (identified with their Jeffries et al. 2001 number in the “Star Number” columns) are listed in Table 5. From the range of conversion factors found, we estimate that the uncertainty on L_{X} due to an inappropriate spectral model is at most 40%, and more typically 12% (rms).

4. OPTICAL IDENTIFICATIONS

In Table 4 we also list optical counterparts to all detected X-ray sources. We have used the optical catalog of Jeffries et al. (2001), complete to about $V = 20$, supplemented by a list of brighter stars, as reported by Jeffries et al. (1997). The Jeffries et al. (2001) catalog number is reported in Table 4 (“Star Number” column). We have identified an X-ray source with an optical star when their distance is $d < 3\Delta r$ (but always $d < 25''$ to avoid many spurious matches in the outer parts of the field of view), to which we have added identifications within $d < 4''$ (but not exceeding $d < 5.5\Delta r$) to allow for residual errors, especially for brighter optical stars (whose optical positions are less accurate) and X-ray sources with very few counts, whose true positional error is underestimated. In doing this, we have also found (and corrected) a systematic offset between optical and X-ray positions of $0''.07$ in R.A. and $0''.19$ in Decl. for stars in Jeffries et al. (2001; slightly larger values of $0''.68$ and $0''.59$ were found for the brighter stars).

In this way, we find that 23 X-ray sources have more than one optical counterpart. Inspecting visually each of these cases, we have found that for most of them one star was a much closer match (within $d < 1.5\Delta r$) than any other candidate counterpart. Therefore, in cases of multiple counterparts we have restricted the matching distance to $d < 1.5\Delta r$. This leaves four X-ray sources with double optical identification (one member and one nonmember for each), with no obvious choice between the two counterparts. These are each listed as two separate rows in Table 4. We have taken the membership information from Jeffries et al. (2001).

To summarize, among the 284 unique X-ray sources we have detected in the NGC 2516 field, we have identified 211 with at least one optical star. There are 155 cluster members associated with an X-ray source and 60 nonmembers associated with an X-ray source (the two numbers sum up to 211+4, the latter being the number of doubly identified sources). There remain 73 X-ray sources without an optical identification with our optical catalog stars. In addition to the detected cluster members, in our combined *Chandra* field of view fall another 570 cluster members not detected in X-rays. Since the total number of members is 1298, there are 573 more members outside our surveyed region. For each of the 570 members that were observed but not detected in any data set, we have computed flux upper limits with PWDetect, in both individual data sets and the all-summed data set. We have then taken the lowest value among the various data sets. The L_{X} upper limits for the undetected cluster members are listed in Table 6.

Taken at face value, we have detected 155/725 cluster members, or 21.4%. However, we caution that our point-source sensitivity varies strongly across the field of view, being much larger near the center, and that Jeffries et al. (2001) estimate some nonmember contamination in their candidate-member catalog, increasing toward the outer parts (i.e., over a large area, where our X-ray sensitivity is poor). This explains in part why this detection fraction is apparently so different from the value of about 42% found

TABLE 5
X-RAY LUMINOSITIES FOR DETECTED NGC 2516 MEMBERS

X-Ray Number	Star Number	$\log L_X$ (ergs s $^{-1}$)	X-Ray Number	Star Number	$\log L_X$ (ergs s $^{-1}$)	X-Ray Number	Star Number	$\log L_X$ (ergs s $^{-1}$)	X-Ray Number	Star Number	$\log L_X$ (ergs s $^{-1}$)
1.....	4125	30.33	67.....	7678	29.74	128.....	8935	29.59	183.....	10894	29.58
2.....	4598	30.30	69.....	7690	29.15	129.....	8967	29.75	185.....	11082	29.53
3.....	15496	29.79	71.....	7743	29.85	130.....	8969	29.07	186.....	11233	30.18
4.....	5024	29.62	72.....	7782	29.77	131.....	8991	29.24	188.....	11485	29.46
5.....	5052	30.09	76.....	7864	30.11	132.....	8997	29.91	190.....	5899	29.48
6.....	5061	29.90	78.....	15503	29.36	133.....	9025	28.99	193.....	7276	29.08
8.....	5957	29.99	81.....	7937	28.94	134.....	9035	29.06	201.....	9402	29.06
9.....	6029	29.99	83.....	7959	29.44	135.....	9048	28.85	202.....	10017	29.24
10.....	6106	29.34	84.....	7962	29.11	137.....	9054	30.03	203.....	10348	28.96
13.....	15499	29.79	85.....	7967	29.25	138.....	9061	29.02	204.....	10871	29.30
14.....	6268	29.38	89.....	8036	29.37	140.....	9140	30.05	211.....	5446	29.47
15.....	6263	29.19	90.....	8047	29.01	141.....	9153	29.35	212.....	6264	29.10
16.....	6373	29.58	91.....	15534	29.25	143.....	9175	29.83	214.....	6751	29.06
17.....	6452	29.40	92.....	8099	29.77	144.....	9185	29.31	215.....	7260	29.19
20.....	6492	29.36	94.....	15504	29.76	145.....	9202	29.07	218.....	4105	30.25
22.....	6570	29.21	95.....	8172	29.18	146.....	9283	28.87	221.....	5862	29.37
23.....	6603	29.25	96.....	8192	29.26	147.....	9286	28.95	222.....	6049	29.33
24.....	6605	29.20	97.....	8261	29.37	149.....	9328	29.58	223.....	6070	29.43
26.....	6640	29.14	100.....	8332	29.36	150.....	9361	29.06	225.....	6508	28.94
27.....	6649	29.94	101.....	8404	29.02	152.....	9465	30.07	226.....	7590	29.01
29.....	6689	29.89	102.....	8408	29.23	154.....	9486	30.03	243.....	11240	29.55
32.....	6852	29.16	106.....	8458	30.09	155.....	9512	29.16	246.....	7358	29.33
33.....	15500	29.88	107.....	8502	29.07	156.....	9676	30.02	252.....	7194	29.03
34.....	7001	29.45	108.....	8529	29.92	158.....	15509	30.53	254.....	7312	28.87
35.....	7104	29.35	110.....	8536	28.98	159.....	15508	30.47	256.....	7454	28.91
37.....	7120	28.70	111.....	8556	28.94	161.....	9835	30.00	259.....	7619	29.35
40.....	7203	28.90	114.....	15506	29.79	162.....	9852	29.52	262.....	8037	29.71
42.....	7231	29.55	115.....	8634	30.05	163.....	9882	29.84	264.....	8126	29.06
44.....	15501	29.44	116.....	8645	30.01	164.....	9908	29.64	266.....	8289	28.75
47.....	15519	28.97	117.....	8647	28.69	165.....	10010	29.14	268.....	8328	28.87
51.....	7419	29.05	118.....	8654	29.08	166.....	10040	29.63	270.....	8411	28.86
52.....	7420	29.25	119.....	8660	29.93	167.....	10046	30.01	273.....	8584	29.39
55.....	7505	28.72	120.....	8737	28.74	169.....	10047	29.75	275.....	8641	29.14
58.....	7553	29.15	121.....	8776	28.92	170.....	10143	30.07	277.....	8689	28.95
60.....	7585	30.13	123.....	8893	29.71	175.....	10471	29.84	278.....	9015	28.87
61.....	7595	29.45	124.....	8886	29.78	178.....	10702	29.18	282.....	9513	29.01
64.....	7622	29.16	125.....	8920	28.85	180.....	10754	29.17	283.....	9655	28.97
65.....	7650	29.57	126.....	8923	28.84	181.....	15510	30.01	284.....	9696	28.96
66.....	7667	29.86	127.....	8932	28.84	182.....	10863	29.40			

by Harnden et al. (2001), who analyzed a subset of the X-ray data used here, considering only the cluster central region (in the same region we find a detection rate of 33.5%), since their input optical catalog (going down to $V \sim 19$) was less complete than the Jeffries et al. (2001) catalog (down to $V \sim 21$) and thus results in 198 observed members in the central region, instead of our 251 observed members. The detailed detection rate for members of various spectral types are reported in Table 7. In this table, the sum of numbers in column (4) is 568, and not 570, since we have left out two (undetected) red giants that are also cluster members according to Dachs (1970). A third red giant member was not observed by us. We note that for all spectral types our detection fraction is lower than 50%. Since optical spectra are not available for most NGC 2516 members, we have assigned spectral types from $B-V$ and $V-I$ optical colors, as listed in the same table, corrected for the average cluster reddening $E(B-V) = 0.12$.

We show in Figure 3 the color-magnitude diagrams for NGC 2516 members and detected nonmembers, using $B-V$ and $V-I$ colors, respectively. The cluster binary sequence is

visible and was discussed by Jeffries et al. (2001). We can see that our detected cluster members span the whole range of colors down to the reddest part of the diagrams. There seems to be a limit around $V \sim 20$, $V-I \sim 3$ to the detected members in the color-magnitude diagram, and this is probably caused by the sensitivity threshold of the X-ray observations. Assuming an X-ray flux threshold $\log f_X \geq 10^{-14.56}$ (ergs s $^{-1}$ cm $^{-2}$), and a bolometric correction $BC = -2.65$, this implies $\log L_X/L_{bol} \geq -3$. This corresponds to the most active dMe stars, and therefore we do not expect to detect in X-rays cluster members fainter than this limit. Some of the nonmembers fall far above the cluster main sequence (but are not cluster giants) and are therefore probable foreground low-mass field stars. A slightly larger number of nonmembers fall below the cluster main sequence and are therefore probable background objects, either active stars or reddened active galactic nuclei (AGNs).

Taking into account the identification radius used for each X-ray source, we have computed the total area searched for matches. Comparing it to the spatial density of stars in the central $10' \times 10'$, we find that the expected

TABLE 6
UPPER LIMITS TO X-RAY LUMINOSITIES FOR UNDETECTED NGC 2516 MEMBERS

Star Number	$\log L_X$ (ergs s $^{-1}$)	Star Number	$\log L_X$ (ergs s $^{-1}$)	Star Number	$\log L_X$ (ergs s $^{-1}$)	Star Number	$\log L_X$ (ergs s $^{-1}$)	Star Number	$\log L_X$ (ergs s $^{-1}$)
1531	30.57	3278	30.26	3961	30.18	4836	29.76	5530	29.38
1645	30.37	3301	30.05	4000	29.94	4840	29.87	5533	29.41
1657	30.41	3387	30.27	4003	30.23	4842	29.87	5536	30.31
1753	30.59	3397	30.15	4046	29.95	4855	29.73	5563	30.27
1781	30.39	3402	30.01	4069	29.84	4889	29.78	5573	29.29
1798	30.44	3406	30.16	4072	29.80	4911	30.43	5576	29.59
1830	30.78	3407	30.28	4089	30.02	4914	29.97	5581	29.80
1832	30.73	3433	30.16	4113	29.91	4915	30.38	5586	29.97
1834	30.55	3440	30.06	4126	30.02	4936	29.75	5626	29.72
1859	30.29	3468	30.64	4146	29.87	5010	29.65	5631	29.64

NOTE.—Table 6 is published in its entirety in the electronic edition of the *Astrophysical Journal*. A portion is shown here for guidance regarding its form and content.

number of chance coincidences is 6.9 for members and 29 for nonmembers. Among members, spurious optical identifications are probably among the redder, fainter stars; for nonmembers, they should be in the “clump” at $V \sim 18$ –20 and $V-I \sim 1$ (see Jeffries et al. 2001). Therefore, our subsample of detected members can be considered nearly free of identification ambiguities, while substantial ambiguities exist for the nonmember detections, which will be paid little attention in the following.

As for the 73 X-ray sources without identification in the Jeffries et al. catalog, we expect that the 8–9 predicted spurious X-ray detections are to be found preferentially among them (the weakest detections fall indeed in this group). We have therefore visually checked whether they are real X-ray sources. While some of them may be spurious, many are certainly not. Then we have examined visually their position on the DSS red images. For 42 of them, there is indeed no visible counterpart down to the plate limit. There are then 10 undefined cases, falling mostly over halos of bright optical stars. Eleven sources have a faint optical starlike counterpart, and another 10 sources have a very faint counterpart, very near to the noise limit (some may indeed be noise). These objects may either be cluster members or unrelated background objects, perhaps extragalactic.

Jeffries et al. (2001) discuss the completeness of their optical catalog, and they expect to be 98% complete down to $V = 19$, and 90% complete for $19 < V < 20$. Therefore, having 155 X-ray-detected cluster members, mostly with $V < 19$, we expect about 3–10 to be missing in the optical catalog. These objects are probably found among those near bright stars, or those with faint DSS counterparts. From the

Chandra deep-survey $\log N - \log S$, and the sensitivity map computed using PWDetect on our combined data set, we estimate that 19–26 extragalactic sources (using the models of Giacconi et al. 2001 and Tozzi et al. 2001, respectively) should be detected in our NGC 2516 fields.

5. RESULTS

5.1. NGC 2516 X-Ray Luminosity Functions

We have computed maximum-likelihood X-ray luminosity functions for all NGC 2516 members observed in our *Chandra* survey, including upper limits, using ASURV (Feigelson & Nelson 1985). We show in Figure 4 these X-ray luminosity functions, separately for the various spectral types. In the same figure, we compare the results obtained for NGC 2516 with those obtained for the Pleiades cluster by Micela et al. (1999) using *ROSAT* HRI data. The Pleiades X-ray luminosities were computed in the band 0.1–2.4 keV, but for the adopted spectral model only a small upward correction (3%–7%) would be needed to convert them to the band 0.1–4.0 keV. The median and mean X-ray luminosities L_X obtained for each spectral types in NGC 2516 are also reported in Table 7. Since we have detected less than 50% of observed members for all spectral types, in some cases (B and A stars) we have only obtained an upper limit on the median L_X .

The B-star X-ray luminosity function spans the widest interval among all spectral types, reaching the highest L_X value found in NGC 2516, or $\log L_X = 30.53$ (ergs s $^{-1}$), and also going down to the lowest detected L_X values and below,

TABLE 7
DETECTION STATISTICS FOR DIFFERENT SPECTRAL TYPES

Spectral Type (1)	Color Range (2)	Number Detected (3)	Number Undetected (4)	Detection Rate (%) (5)	Median $\log L_X$ (ergs s $^{-1}$) (6)	Mean $\log L_X$ (ergs s $^{-1}$) (7)
B	$(B-V)_0 < 0.0$	12	26	31.6	<28.54	29.00
dA	$0.0 \leq (B-V)_0 < 0.3$	12	46	20.7	<28.51	28.88
dF	$0.3 \leq (B-V)_0 < 0.5$	19	25	43.2	29.40	29.41
dG	$0.5 \leq (B-V)_0, (V-I)_0 < 0.93$	38	77	33.0	29.06	29.18
dK	$0.93 \leq (V-I)_0 < 2.2$	52	175	22.9	29.02	29.07
dM	$2.2 \leq (V-I)_0 < 5.0$	22	219	9.1	28.69	28.74

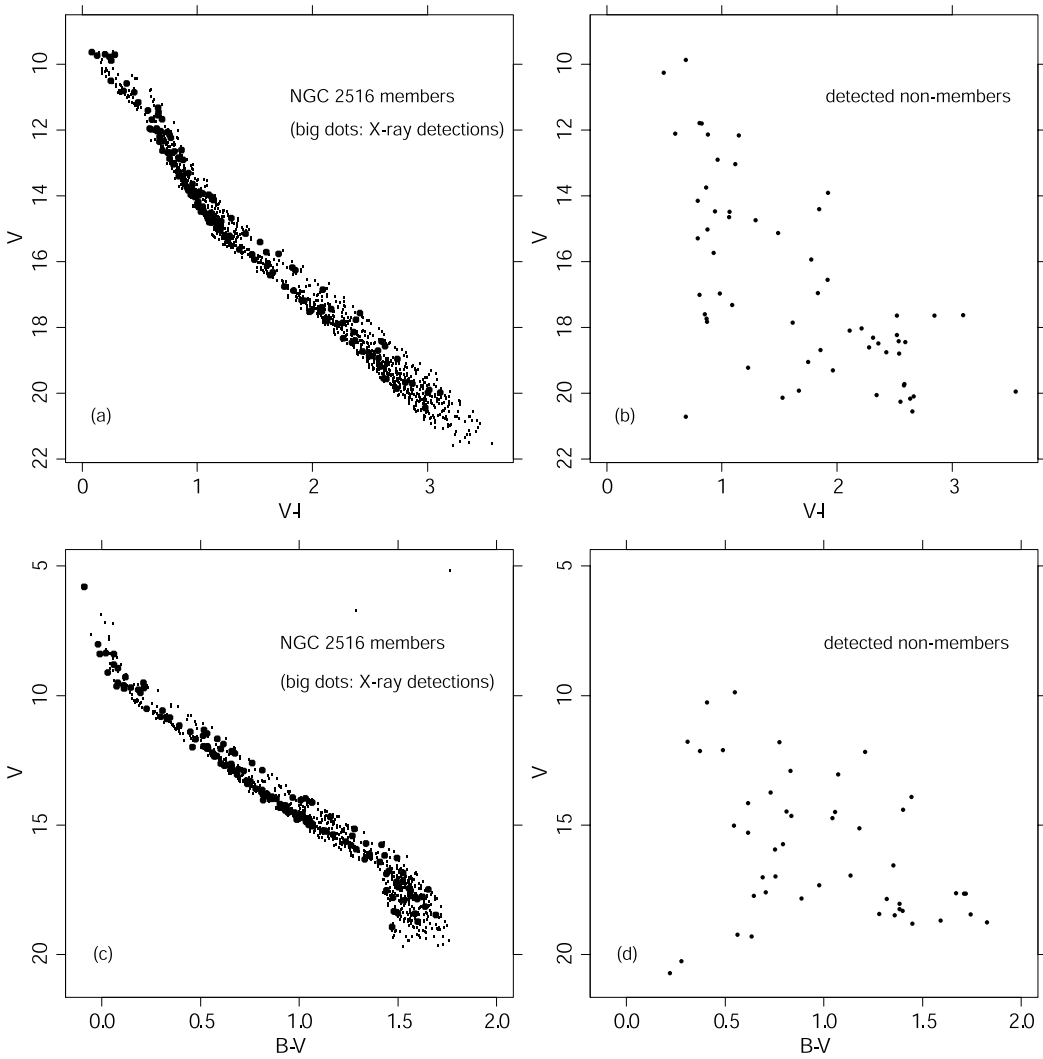


FIG. 3.—(a) (V , $V-I$) Color-magnitude diagram for NGC 2516 members, with detected members marked as big dots. Since the $V-I$ color of the brightest stars is not available, they are missed in this plot. (b) (V , $V-I$) Color-magnitude diagram for nonmembers detected as X-ray sources in our *Chandra* data. A few among them fall in the same region as NGC 2516 members but have a $B-V$ color incompatible with membership. Faint, relatively blue objects may well be extragalactic. (c) (V , $B-V$) Color-magnitude diagram for NGC 2516 members, with detected members marked as big dots. This diagram includes all brighter members. (d) (V , $B-V$) Color-magnitude diagram for detected nonmembers.

with many stars undetected with upper limits lower than $\log L_X = 29.0$ (ergs s^{-1}). The emission of the two X-ray brightest B stars cannot therefore be due to lower-mass companions but must be intrinsic to the massive stars themselves (of types B9.5 V and B2 IVnpe, respectively), as concluded already by Jeffries et al. (1997), and is probably due to shocks in the stellar wind, as usually found in OB stars.

The A-star X-ray luminosity function spans instead a range similar to the luminosity functions of later-type stars and is compatible with an X-ray emission uniquely due to lower-mass companions. The A stars have the second lowest detection rate in our NGC 2516 survey (see Table 7); only M stars have a lower detection fraction, owing to both their intrinsic X-ray faintness and to strong nonmember contamination in their optical catalog. However, NGC 2516 is remarkable in having a number of chemically peculiar A stars as members. We have observed eight of them, and detected six or seven (because of the unresolved double CPD-60 944), namely, one-half of our detected A stars are chemically peculiar. Therefore, either there is a connection

between chemical peculiarity and binarity, such that peculiar stars are more often binaries than nonpeculiar stars, and the X-ray emission comes from the companions, or rather a connection exists between chemical peculiarity and X-ray activity intrinsic to the A stars themselves, without emission from companions. This is likely to happen if these peculiarities go as far as to modify the structure of the outer layers of the star, e.g., changing the opacity and turning convection on (many such stars are known to possess strong surface magnetic fields; Borra, Landstreet, & Mestel 1982). Drake et al. (1994) have also found evidences of strong X-ray emission from chemically peculiar early-type stars. In NGC 2516, the very high X-ray detection rate of chemically peculiar A stars, especially compared to the low detection rate of normal A stars, is an intriguing result that surely deserves careful separate investigations.

Among the three red giants belonging to NGC 2516, two are in our observed sample, but neither was detected. The first of these stars has $V = 6.71$, $B-V = 1.28$, and $\log L_X < 28.73$ (ergs s^{-1}), and the other $V = 5.19$, $B-V =$

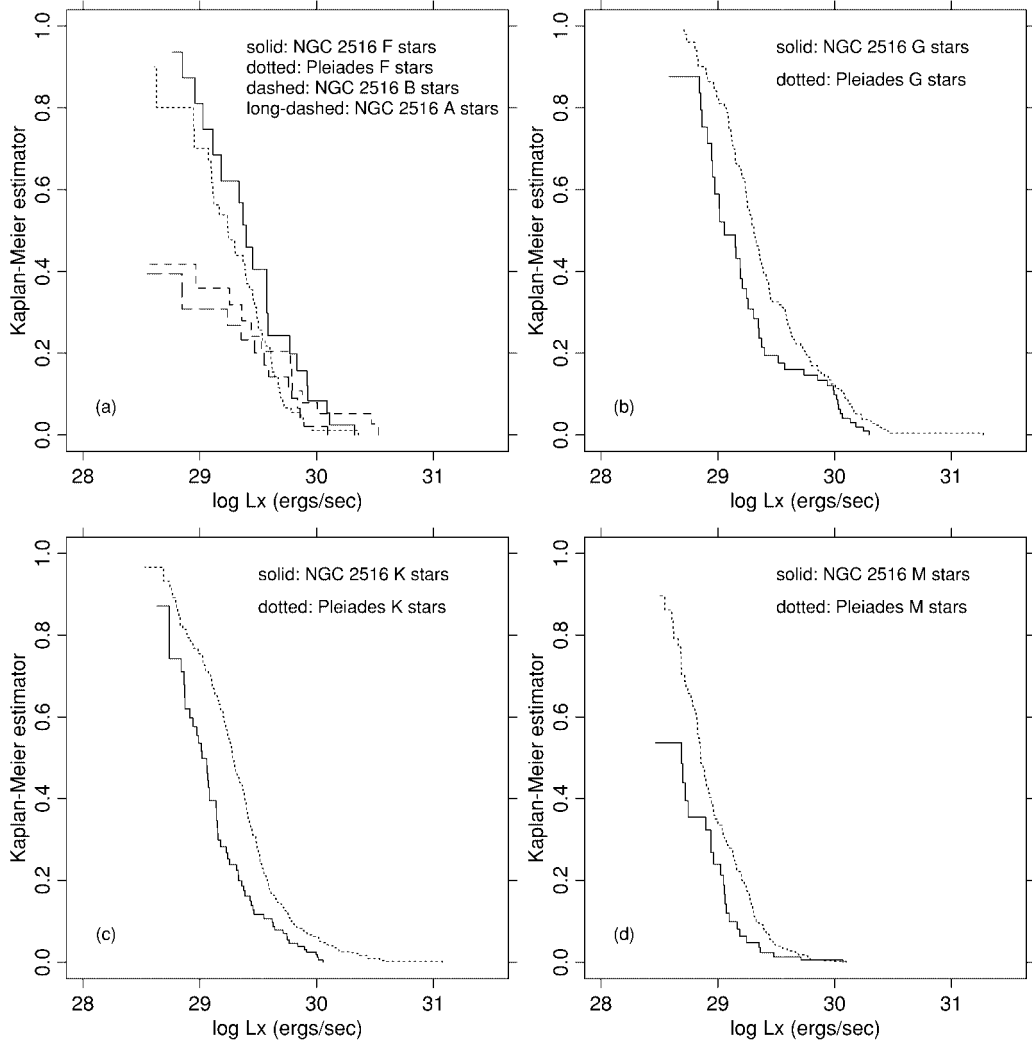


FIG. 4.—Maximum-likelihood X-ray luminosity functions for NGC 2516, separately for different spectral types (not corrected for contaminants), and comparison with analogous luminosity functions for the Pleiades (from Micela et al. 1999). (a) Solid line: NGC 2516 F stars; dotted line: Pleiades F stars; dashed line: NGC 2516 B stars; long-dashed line: NGC 2516 A stars. (b) Solid line: NGC 2516 G stars; dotted line: Pleiades G stars. (c) Solid line: NGC 2516 K stars; dotted line: Pleiades K stars. (d) Solid line: NGC 2516 M stars; dotted line: Pleiades M stars.

1.76, and $\log L_X < 29.99$ (ergs s^{-1}). They are not included in the X-ray luminosity functions discussed below.

As shown in Table 7, the F stars in NGC 2516 have both a median L_X and a detection fraction larger than other spectral types. For this reason, we can conclude that the X-ray emission of F stars is very probably intrinsic and not due to companions. For later types, we see a steady decrease in the median L_X toward lower masses. In Figure 4 we see also that for G and K stars the NGC 2516 luminosity functions stay distinctly below the corresponding luminosity functions for the Pleiades, a result similar to that found by Jeffries et al. (1997), Harnden et al. (2001), and Sciortino et al. (2001) but with better detection statistics. For M stars, we find a slightly lower luminosity function with respect to the Pleiades, analogously to Sciortino et al. (2001), while Harnden et al. (2001) derived a luminosity function very similar to the Pleiades. Jeffries et al. (1997) argued that the lower activity level in NGC 2516 was probably due to its lower metallicity compared to the Pleiades and discussed how metallicity can lower X-ray activity especially during some evolutionary phases. A more recent work (Terndrup et al. 2002), however, seems to rule out a subsolar metallicity

for NGC 2516, so that this can no longer be a valid explanation for the observed lower activity levels in NGC 2516. Although NGC 2516 is older than the Pleiades, it is unclear if the observed, fairly strong, decrement in the average X-ray luminosities can be uniquely attributed to an age difference. Nor is the age-activity relation without exceptions, as is shown by the Hyades and Praesepe clusters, having the same age but different X-ray luminosity functions. Thus, NGC 2516 might be another discrepant case with respect to the average age-activity relation. Before drawing such a conclusion, however, we must still ascertain whether some bias affects the X-ray luminosity functions just derived for NGC 2516. One such bias might easily be the contamination by nonmembers in the optical catalog. The magnitude of such a contamination was estimated by Jeffries et al. (2001), and we try to eliminate its effect on the X-ray luminosity functions in the next section.

5.2. Nonmember Contamination

We assume that contaminating nonmembers are found among undetected stars in the optical NGC 2516 catalog, since X-ray-detected candidate members can be considered

confirmed members. Jeffries et al. (2001) tabulate estimates of the nonmember contamination fraction affecting their catalog, separately for different $V-I$ ranges, and for single and binary stars, respectively. On this basis, we have computed, for each stellar color/type range, the number of expected contaminants and, therefore, the probability p_m that a star is actually a member. A given upper limit was then included in the luminosity function if, taking a random number from a uniform distribution between 0 and 1, this was smaller than the membership probability p_m for that star. This procedure was repeated 200 times for each luminosity function, again separately for different spectral types (Fig. 5). These simulated luminosity functions should be a good estimate of the true, contamination-free NGC 2516 luminosity function. A few caveats apply, however: the Jeffries et al. (2001) contamination estimates are averaged over the whole optical survey. The contamination is lower near cluster center and higher outside our X-ray-surveyed region; therefore, our correction may be slightly overestimated.

In Figure 5 we see that the correction is negligible for F stars, whose contamination is expected to be very small. For G stars the correction is more noticeable, and the G-star

NGC 2516 luminosity function may even cross that of the Pleiades around $\log L_X = 30$ (ergs s^{-1}). Its median value, however, remains lower, albeit by only 0.13 dex. Also in K stars, the discrepancy with the Pleiades is slightly reduced with respect to the uncorrected case, but it remains very evident and, in fact, the largest among all spectral types. A set of two-sample Wilcoxon tests, applied to the Pleiades and to each of the simulated luminosity functions, gives a distribution of probabilities of not being drawn from the same population, with median value $P_{50} = 0.885$, 18% quantile $P_{18} = 0.884$, and 82% quantile $P_{82} = 0.891$, for F stars. For G stars, we obtain $P_{50} = 0.954$, $P_{18} = 0.921$, and $P_{82} = 0.971$, and for K stars $P_{50} = 0.999$, $P_{18} = 0.998$, and $P_{82} = 0.999$. Therefore, only in the case of K stars are the NGC 2516 and Pleiades luminosity functions different more significantly than 99.7% (3σ).

In NGC 2516 M stars the contamination is large and the correction to the luminosity function quite relevant. The corrected median L_X may even be the same as the Pleiades, and the whole luminosity function of NGC 2516 M stars does not differ substantially from that of Pleiades M stars. A Wilcoxon test gives $P_{50} = 0.962$, $P_{18} = 0.942$, and $P_{82} = 0.978$, a not very significant difference. Qualitatively, this is

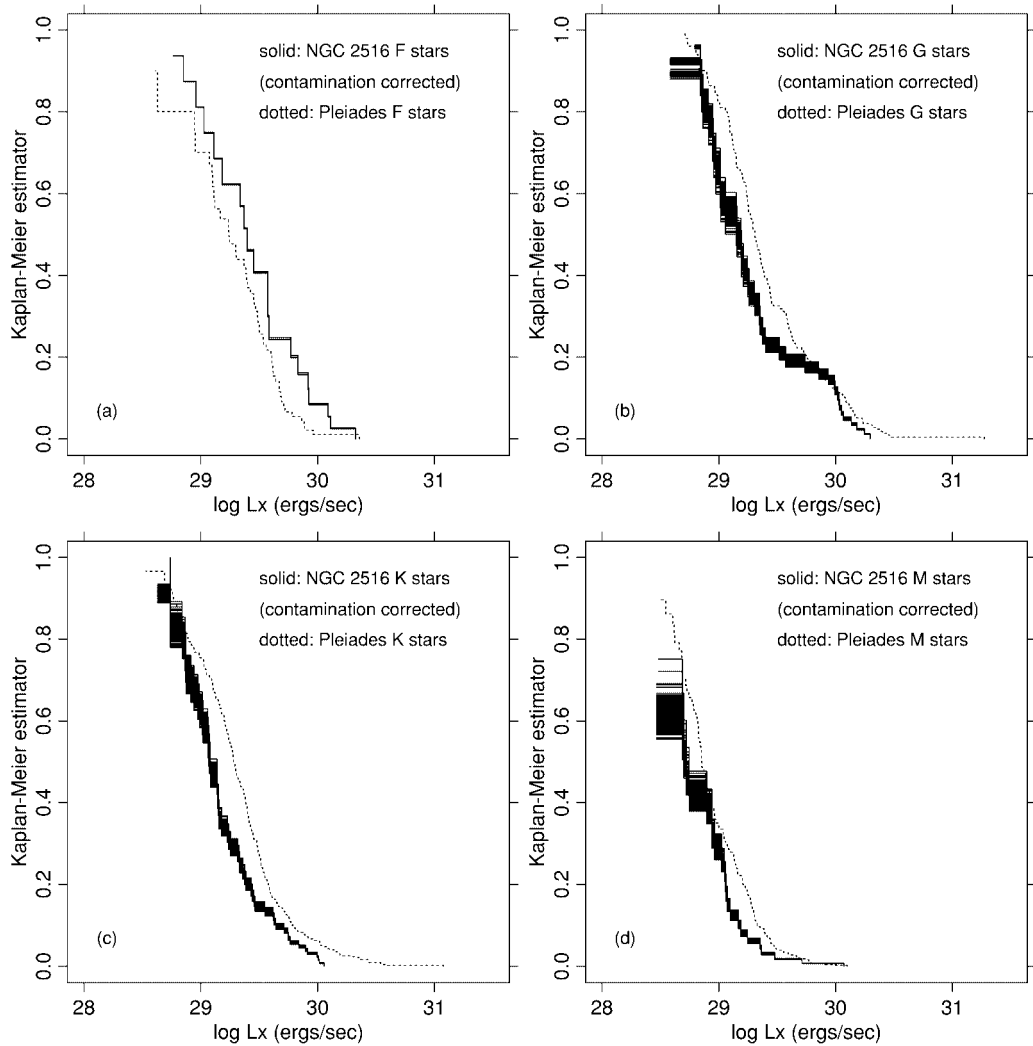


FIG. 5.—X-ray luminosity functions for NGC 2516 (solid lines), separately for different spectral types, corrected statistically for nonmember contamination (see text). Each luminosity function was simulated 200 times. Also shown for comparison are the Pleiades luminosity functions (dotted lines). After correction, only the NGC 2516 K star luminosity function remains significantly different from its analog in the Pleiades. (a) F stars; (b) G stars; (c) K stars; (d) M stars.

TABLE 8
CONTAMINATION-CORRECTED AVERAGE X-RAY LUMINOSITIES

SPECTRAL TYPE	MEDIAN $\log L_X$ (ergs s $^{-1}$)			MEAN $\log L_X$ (ergs s $^{-1}$)			PROBABILITY OF DIFFERENCE WITH RESPECT TO PLEIADES		
	18%	50%	82%	18%	50%	82%	18%	50%	82%
dF	29.40	29.40	29.40	29.41	29.41	29.41	0.884	0.885	0.891
dG	29.16	29.16	29.19	29.23	29.25	29.27	0.921	0.954	0.971
dK	29.07	29.08	29.08	29.13	29.14	29.15	0.998	0.999	0.999
dM.....	28.70	28.72	28.72	28.77	28.78	28.80	0.942	0.962	0.978

the same result found by Micela et al. (2000) using *ROSAT* HRI data and by Harnden et al. (2001) using a subset of our *Chandra* data. The median and mean values of the L_X distributions corrected for contaminations are listed in Table 8.

We conclude that, at least in the case of K stars, there is a definite lower X-ray activity level in NGC 2516 with respect to the Pleiades that cannot be ascribed to contamination by stars not belonging to the cluster. If Jeffries et al. (2001) underestimate the optical contamination, however, the X-ray luminosity functions move toward higher values and become more similar to the Pleiades. An underestimate by a factor of 2 would result in a probability of difference of $P_{50} = 0.766$ for the G stars, of $P_{50} = 0.977$ for the K stars, and of $P_{50} = 0.730$ for the M stars.

We have also investigated how much these results depend on the assumed distances for NGC 2516 and the Pleiades. For these latter, we have adopted a distance of 127 pc, as in Micela et al. (1999). The NGC 2516 distance used here, 387 pc, is the same used by Jeffries et al. (1997) and coincides also with that derived by Terndrup et al. (2002) from variable-metallicity isochrone fitting. For both clusters, the *Hipparcos* distances are smaller: 116 pc for the Pleiades (Mermilliod et al. 1997) and 346 pc for NGC 2516 (Robichon et al. 1999). If we adopt the *Hipparcos* distances for both clusters, then their X-Ray luminosity functions shift toward lower values by 0.079 dex for the Pleiades, and by 0.097 dex for NGC 2516, respectively. Therefore, they become more similar for F stars and more different for G, K, and M stars. The contamination-corrected probabilities of difference P_{50} for G, K, and M stars now become 0.976, 0.99956, and 0.984, respectively. Again, the only very significant difference occurs for K stars. If a fixed metallicity value for NGC 2516 (from spectroscopy) is instead used, Terndrup et al. (2002) derive a larger distance of 407 pc. Using this distance value (and assuming 127 pc for the Pleiades), the NGC 2516 luminosity functions move upward by 0.045 dex. In this case, the F-star luminosity functions become more different, and those of G, K, and M stars more similar. The contamination-corrected probabilities of difference P_{50} for G, K, and M stars are in this case 0.842, 0.985, and 0.840, respectively, and the K-star difference thus becomes only marginally (2.44σ) significant. This larger distance value for NGC 2516 might be unreliable, however, being incompatible at the 2.5σ level with the *Hipparcos* distance (Terndrup et al. 2002), while the value of 387 pc, used in this paper, is well compatible with the *Hipparcos* value.

5.3. X-Rays and Binarity

In the color-magnitude diagram of NGC 2516, a binary sequence is easily identifiable (Fig. 3), and on this basis

Jeffries et al. (2001) have assigned a binarity flag to photometric NGC 2516 members. By definition, the binary sequence comprises only near-equal mass systems ($q > 0.6$), so that more binaries with larger mass ratios are left among the apparently single stars.

We have examined whether the NGC 2516 binaries have an enhanced emission with respect to single stars that may be due to some interaction between close components, as in well-known active binaries. The detection rate of F and G binaries (taken together to augment their statistics) is of $18/55 = 0.327$, while the rate for single F and G stars is $39/104 = 0.375$. For K binaries the rate is $14/58 = 0.241$, while for single K stars is $38/169 = 0.225$. Therefore, differences between detection rates of singles and binaries of the same type are negligible. This is surprising, since if there is a given probability P_1 of detecting a single star of a given type, the probability of detecting at least one star in a pair, of the same type, should be larger: $P_2 = 1 - (1 - P_1^2) = P_1(2 - P_1)$. Thus, in the case of K binaries one would expect a detection fraction of 0.40. A possible explanation for this apparent lack of detected binaries might be a different contamination fraction for singles and binaries, respectively. Also a different spatial distribution might produce the same effect, if for example the binaries are less concentrated toward the center and thus observed at large off-axis angles (and therefore lower sensitivity) in our X-ray data sets; however, the mean distances from cluster center of singles and binaries are 17.7 and 19.2 , respectively, and their small difference seems not enough to account for the observed effect. On the contrary, mass segregation (confirmed by Jeffries et al. 2001) would lead us to expect more binaries near the center. A better explanation may be that the singles are not actually singles, and companions with much lower optical luminosity contribute a nonnegligible fraction to the detected X-ray flux. In fact, using field stars' q distributions, Jeffries et al. (2001) estimated the total percentage of binaries in NGC 2516 to be high ($\sim 85\%$), although probably no higher than in the Pleiades.

It is also interesting to study the luminosity functions of binary versus single stars, as we show in Figure 6 separately for F and G stars and for K stars. We plot the binary star function, the single star function (both corrected for contamination), and the convolution of the latter with itself, simulating a binary star luminosity function. The observed F and G binary luminosity function crosses the simulated binary luminosity function with a high-activity tail independent of any contamination correction. This is probably due to close binaries, making up a sizable fraction of our binary sample, which have not yet slowed down their rotation (as single F, G stars have done) and are therefore more active than either wide binaries or pairs of single stars.

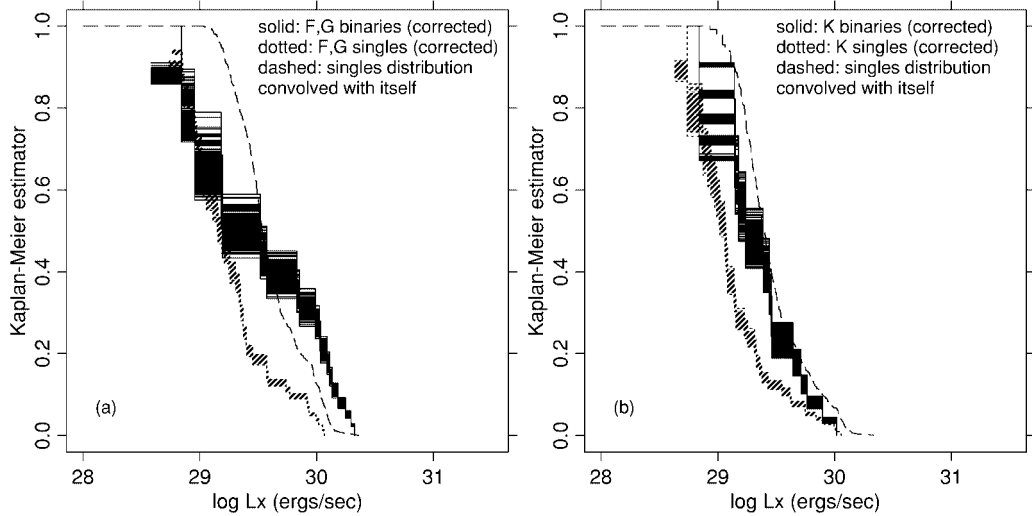


FIG. 6.—Comparison of (photometric) single- (dotted lines) and binary-stars (solid lines) X-ray luminosity functions (contamination-corrected), and the convolution of the single-star distribution with itself (dashed lines). (a) F and G stars; (b) K stars.

In the case of K stars, the contamination correction is critical to bring the observed binary star luminosity function close to the simulated one. If the largest correction is adopted, the observed and simulated binary stars luminosity functions are very similar, suggesting that binarity does not affect X-ray emission. On the contrary, if no correction is made, one would conclude that K binaries are underactive with respect to single K stars. This might not be a real effect, however, but simply caused by apparently simple stars, which are actually binaries with large mass ratios. We conclude that, at most, K binaries in NGC 2516 are only slightly underactive with respect to their single counterparts.

In the Pleiades, the X-ray luminosity function of binary G stars is consistent with the convolution of that of single G stars with itself (Micela et al. 1996), and the same is found for K stars. Binary stars in the Pleiades are known much better than in NGC 2516, and our findings do not rule out that binaries in NGC 2516 behave in the same way as

Pleiades binaries (apart from the high-activity tail in the NGC 2516 F,G binaries). In the older Hyades, Pye et al. (1994) found the opposite effect for dK stars, namely, long-period binary stars are significantly more active than pairs of single dK stars, a behavior that we can rule out for NGC 2516 dK stars.

5.4. Relationships between X-Ray and Optical Properties

In addition to the study of color-dependent X-ray luminosity functions, we have examined possible further relationships between X-ray emission and optical colors (hence stellar mass). Plots of $\log f_X/f_V$ versus $V-I$ are shown in Figures 7a and 7b, for members and nonmembers, respectively. As observed in other clusters, there is a clear trend of increasing $\log f_X/f_V$ from the bluest to the reddest colors (Fig. 7a). In this figure, the most massive stars are not included since we lack their $V-I$ colors. The total observed range of $\log f_X/f_V$ (including the massive stars) is

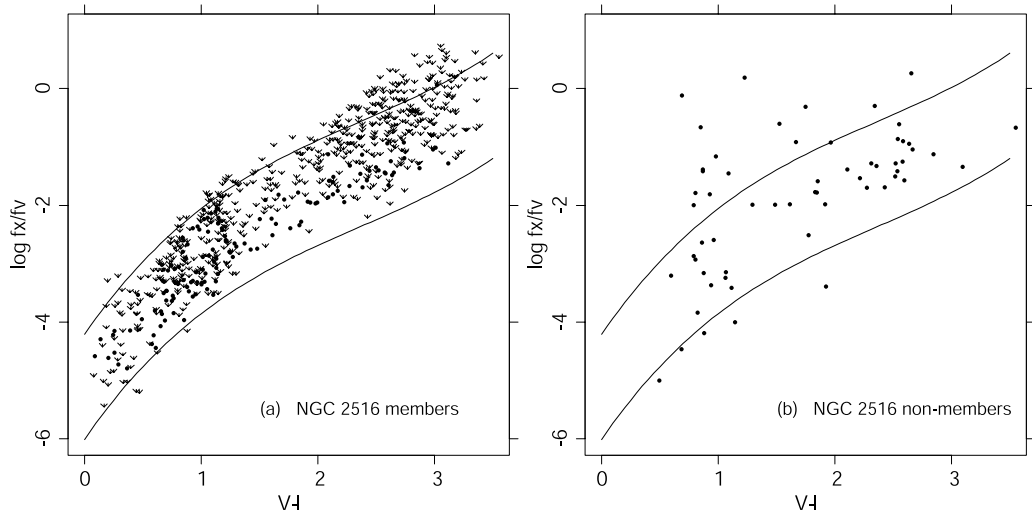


FIG. 7.—Plot of $\log f_X/f_V$ vs. $V-I$ color, for (a) NGC 2516 members and (b) detected nonmembers. Many nonmembers fall in the same region as cluster members and may be active young stars. Other objects have a much larger f_X/f_V for their $V-I$ and are probably noncoronal sources.

[-5.35 , $+0.066$]. Values of $\log f_X/f_V \sim 0$ are rather extreme and attained only by a few flaring M stars; more common “high” values of $\log f_X/f_V$ cluster around $\log f_X/f_V \sim -1$, also attained by the latest-type (dM) stars in our sample. The low $\log f_X/f_V$ values that we observe for the most massive stars are also in agreement with those typical of B stars. For a given color, there is a large spread, by 1 order of magnitude or more, as is especially evident for G-early K stars ($V-I \sim 1$). Upper limits are in most cases consistent with the distribution of detections and do not imply a different population of low-activity stars.

Since both $V-I$ and $\log f_X/f_V$ are (to a first approximation) distance-independent quantities, we can meaningfully compare their distribution for members and nonmembers. We have selected in Figure 7a a region where all cluster members are found and have overplotted this region in Figure 7b. Here we see that some objects fall in the same region as cluster stars and are therefore compatible with coronally active, probably young stars (some of them might actually be misclassified real cluster members). Young active stars are expected to be found around this sky direction, belonging to the Gould Belt (Guillout et al. 1998). Other objects are either over- or underluminous in X-rays for their optical colors, and they may be distant AGNs or nearby unactive stars, respectively (or simply spurious identifications). This diagram may help to reject spurious identifications with cluster members (that however seem not to be present in our sample) but cannot be used to select new cluster members blindly, without risking to include coronally active stars not belonging to the cluster. One possible exception is that of stars passing the color-magnitude selection in Jeffries et al. (2001) but not their two-color test (e.g., because of unrelated companions or weak cosmic rays). We have therefore checked where such stars fall in Figure 7b and have found only three stars in the “acceptable” cluster region, having $1.0 \leq V-I \leq 1.5$. These are indeed good candidate cluster members. However, their number is so small that our conclusions remain unaffected.

5.5. X-Rays and Rotation

On the basis of the newly available rotational data (Terndrup et al. 2002), we have made a plot of L_X versus $v \sin i$, as shown in Figure 8. Unfortunately, $v \sin i$ is available for only 33 X-ray-detected stars in our sample (two F stars, 26 G stars, and five K stars), plus 18 undetected stars (one A star, five F stars, 11 G stars, and one K star). Although there is not a tight correlation in these NGC 2516 data, the cloud of points for NGC 2516 follows rather well the relation $\log L_X = 27 + 2 \log(v \sin i)$, found by Pallavicini et al. (1981) for late-type coronal sources (also plotted in Fig. 8). The four upper limits at $\log v \sin i > 1.5$, clearly lower than the Pallavicini et al. relation, are all F stars. Here, we have split the observed L_X among components of equal-mass binary pairs (crosses in Fig. 8), which gives a better agreement with the Pallavicini relation, albeit with a factor of ~ 3 scatter (as stated in § 5.3, some apparently single stars may actually be doubles as well). Therefore, it appears that NGC 2516 is not characterized by a peculiar dynamo mechanism acting in its stars, although this needs to be confirmed by more rotational data. Therefore, any dissimilarity with the Pleiades should be traced back to a dissimilarity in the rotational period distributions of the two clusters. Such a difference has indeed been found and

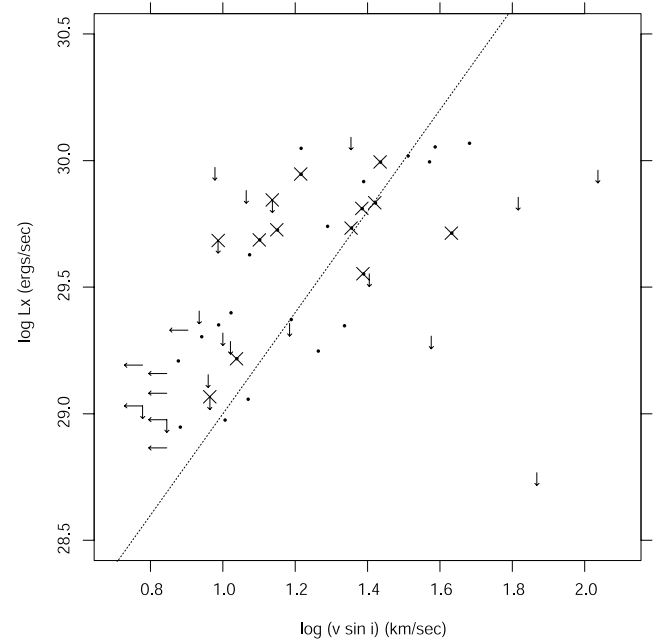


FIG. 8.—Plot of L_X vs. $v \sin i$ for NGC 2516 members. Binaries are indicated with crosses, and their X-ray luminosity was divided by two in this plot. Also indicated is the Pallavicini et al. (1981) relation (dotted line). Most points in this plot are G stars. The four discrepant upper limits at large $v \sin i$ are all F stars.

discussed by Terndrup et al. (2002), who consider it in agreement with the known age difference between these clusters.

6. CONCLUSIONS

We have performed a comprehensive analysis of the *Chandra* imaging observations of the young cluster NGC 2516, studying both individual data sets and their combination, to achieve the highest sensitivity. Near cluster center, we detect cluster members with fluxes down to $\log f_X = -14.56$ (ergs s^{-1} cm^{-2}), or $\log L_X = 28.69$ (ergs s^{-1}). Minimum detectable fluxes in the deepest individual data sets are about a factor of 1.25–1.7 higher. The limiting X-ray luminosities reached by previous studies were $\log L_X \sim 29.0$ (ergs s^{-1}) (Jeffries et al. 1997), $\log L_X \sim 29.3$ (ergs s^{-1}) (Micela et al. 2000), and $\log L_X \sim 28.65$ (ergs s^{-1}) (Harnden et al. 2001; Sciortino et al. 2001). We detect 284 unique X-ray sources, of which 155 identified with candidate cluster members from optical photometry. Thanks to the narrow *Chandra* PSF there is no ambiguity in the optical identifications, except for a handful of cases.

The detection rate as a function of spectral type is lowest for A and M stars (the latter, however, being contaminated by nonmembers) and is maximum for F stars but never reaches 50%. We have attempted to evaluate the contamination for the different stellar types and have built contamination-corrected X-ray luminosity functions that differ significantly from the uncorrected distributions for G and later-type stars.

B stars show a large variety of X-ray luminosities, from strong emission to nondetection with low upper limits. The X-ray emission of the brightest B stars is not compatible with emission from lower-mass companions. The X-ray emission found (occasionally) in A stars is instead compatible with this hypothesis, but it remains unexplained why

among these stars we detect nearly all chemically peculiar stars and very few normal A stars.

The K stars X-ray luminosity function, corrected for contaminations, is significantly lower than the corresponding one in the Pleiades. This may be due in part to the (observed) reduced rotation rates of NGC 2516 stars with respect to their Pleiades analogs, but it is unclear if this may account for the whole difference. Less significant differences (around 2σ level) are found instead in the luminosity functions of G and M stars (slightly lower in NGC 2516 than in the Pleiades) and of F stars (slightly higher in NGC 2516 than in the Pleiades).

At least some among binary F and G stars in NGC 2516 are overactive with respect to single F and G stars. Instead, NGC 2516 K binaries seem slightly underactive compared to single K stars, but the significance of this result depends much on the selection of an uncontaminated member/binary sample.

The reduced X-ray activity level in the G and K stars in NGC 2516 was already observed using previous X-ray data, and it was attributed to a presumed low metallicity of NGC

2516 stars. Recent studies have derived instead solar-like abundances for NGC 2516 and have left only the small age difference between this cluster and the Pleiades as the most plausible reason to explain their different X-ray emission. Also, the dependence of X-ray emission on stellar rotation for NGC 2516 stars appears quite normal.

The sample of NGC 2516 stars for which detailed optical spectra are now available, however, is rather small, and limited to early-G at the latest, while K stars show the largest discrepancy of X-ray activity levels with the Pleiades. As remarked by Terndrup et al. (2002), spectra of these later-type stars, on which a more complete study may be based, will be obtainable using telescopes of the 8–10 m class, which are just now becoming available.

F. D., E. F., G. M., and S. S. acknowledge support from the Italian ASI and MIUR. S. J. W. acknowledges support from the *Chandra* X-Ray Center under NASA contract NAS8-39073. We all are grateful to the *Chandra* staff for the achievements made possible by this mission.

REFERENCES

- Borra, E. F., Landstreet, J. D., & Mestel, L. 1982, *ARA&A*, 20, 191
 Dachs, J. 1970, *A&A*, 5, 312
 Dachs, J., & Hummel, W. 1996, *A&A*, 312, 818
 Damiani, F., Maggio, A., Micela, G., & Sciortino, S. 1997a, *ApJ*, 483, 350
 —. 1997b, *ApJ*, 483, 370
 Drake, S. A., Linsky, J. L., Schmitt, J. H. M. M., & Rosso, C. 1994, *ApJ*, 420, 387
 Feigelson, E. D., & Nelson, P. I. 1985, *ApJ*, 293, 192
 Flaccomio, E., Damiani, F., Micela, G., Sciortino, S., Harnden, F. R., Murray, S. S., & Wolk, S. J. 2003, *ApJ*, 582, 382
 Gagné, M., Caillault, J.-P., & Stauffer, J. R. 1995, *ApJ*, 450, 217
 Giacconi, R., et al. 2001, *ApJ*, 551, 624
 Guillout, P., Sterzik, M. F., Schmitt, J. H. M. M., Motch, C., & Neuhauser, R. 1998, *A&A*, 337, 113
 Harnden, F. R., Jr., et al. 2001, *ApJ*, 547, L141
 Jeffries, R. D., Thurston, M. R., & Hambly, N. C. 2001, *A&A*, 375, 863
 Jeffries, R. D., Thurston, M. R., & Pye, J. P. 1997, *MNRAS*, 287, 350
 Mermilliod, J.-C. 1981, *A&A*, 97, 235
 Mermilliod, J.-C., Turon, C., Robichon, N., Arenou, F., & Lebreton, Y. 1997, in *Hipparcos* Venice '97, ed. B. Battrick & M. A. C. Perryman (ESA SP-402; Noordwijk: ESA), 643
 Micela, G., Sciortino, S., Jeffries, R. D., Thurston, M. R., & Favata, F. 2000, *A&A*, 357, 909
 Micela, G., Sciortino, S., Kashyap, V., Harnden, F. R., Jr., & Rosner, R. 1996, *ApJS*, 102, 75
 Micela, G., et al. 1999, *A&A*, 341, 751
 Pallavicini, R., Golub, L., Rosner, R., Vaiana, G. S., Ayres, T., & Linsky, J. L. 1981, *ApJ*, 248, 279
 Pye, J. P., Hodgkin, S. T., Stern, R. A., & Stauffer, J. R. 1994, *MNRAS*, 266, 798
 Robichon, N., Arenou, F., Mermilliod, J.-C., & Turon, C. 1999, *A&A*, 345, 471
 Sciortino, S., et al. 2001, *A&A*, 365, L259
 Snowden, M. S. 1975, *PASP*, 87, 721
 Terndrup, D. M., Pinsonneault, M., Jeffries, R. D., Ford, A., Stauffer, J. R., & Sills, A. 2002, *ApJ*, 576, 950
 Tozzi, P., et al. 2001, *ApJ*, 562, 42
 Wolk, S. J., et al. 2002, *ApJ*, submitted